Forschungszentrum Karlsruhe
in der Helmholtz-Gemeinschaftt

Wissenschaftliche Berichte
FZKA 7232

Stresses in Oxidizing Tubes: An Analytical Solution of the Stress-strain Equations

H. Steiner, M. Heck, J. Konys

Institut für Materialforschung
Programm Nukleare Sicherheitsforschung

Juni 2006

Forschungszentrum Karlsruhe

in der Helmholtz-Gemeinschaft

Wissenschaftliche Berichte

FZKA 7232

Stresses in oxidizing tubes: An analytical solution of the stress-strain equations

H. Steiner, M. Heck, J. Konys

Institut für Materialforschung

Programm Nukleare Sicherheitsforschung

Forschungszentrum Karlsruhe GmbH, Karlsruhe

2006

Forschungszentrum Karlsruhe GmbH
Postfach 3640, 76021 Karlsruhe

Mitglied der Hermann von Helmholtz-Gemeinschaft
Deutscher Forschungszentren (HGF)

ISSN 0947-8620

urn:nbn:de:0005-072320

Spannungen in oxidierten Rohren: Eine analytische Lösung der Spannungs-Dehnungsgleichungen.

Zusammenfassung

Wenn metallische Komponenten in korrosiven Medien betrieben werden, wird ihre Lebensdauer im Allgemeinen durch das Vorhandensein von Schutzschichten bestimmt, da sie als Barrieren wirken. Durch die Volumenänderung aufgrund der Oxidation können sich im Material beträchtliche Spannungen aufbauen, die so genannten Wachstumsspannungen. Diese mechanischen Spannungen können zur Rissbildung in der Oxidschicht und sogar zu Abplatzungen derselben führen.

Zur Berechnung der Wachstumsspannungen in oxidierenden Rohren wurde ein visko-elastisches analytisches Spannungsmodell entwickelt. Es können dabei sowohl ein-axiale als auch mehr-axiale Spannungstensoren behandelt werden, desgleichen verschiedene Ausprägungen der Oxidation wie Oberflächen- und Grenzflächen-Oxidation sowie Bildung von Doppelschichten. Es ergibt sich, dass sogar relativ kleine Werte für die lateralen Komponenten des Oxidations-Tensors zu großen Spannungseffekten führen können.

Eine vereinfachte Version des Models wurde zur Berechnung der bei Hüllrohren aus Zry auftretenden Dehnungen angewandt, die unter Luft oxidiert wurden. Das Auftreten von lateralen Oxidations-Dehnungen war hierbei der entscheidende Effekt.

Abstract

When metallic components operate in aggressive environments their service life is, in general, determined by the presence of a protective surface film which acts as a barrier to the reactants. Large residual stresses can result from the volume changes due to oxidation, the so-called growth stresses. These stresses may lead to film cracking or spalling or both.

A visco-elastic model for the calculation of growth stresses in oxidizing tubes has been developed. It can deal with uniaxial and multi-axial oxidation strain tensors. Different oxidation modes like surface and interface oxidation as well as duplex scale formation are treated. It appears that even relatively small lateral oxidation strain components could have a considerable effect on the stress level in the tube.

A simplified version of the model has been applied to simulate the geometrical changes of Zry tube sections exposed to air having reached the break-away regime. We think that lateral oxidation strains were mainly responsible for the observed diameter increase.

Contents

List of tables

List of figures

Nomenclature

		Subscripts and Superscripts	
E	Young's modulus	av	average
Φ	Pilling-Bedworth ratio	cl	cladding
ν	Poisson ratio	d	displaced
e	oxidation strain	el	elastic
ε	total strain	eq	equivalent
σ	stress	f	oxide film
δ	scale thickness	i	inner
cr	creep	inel	inelastic
h	thickness	int	interface
r	radius	intr	intrinsic
u	displacement	lat	lateral
		me	metal
		o	outer
		ox	oxide
		par	parabolic
		r	radial
		s	metallic substrate
		tot	total
		z	axial
		Θ	azimuthal

1. Introduction

When metallic components operate in aggressive environments their service life is, in general, determined by the presence of a protective surface film which acts as a barrier to reactants, as, for example, in Lead-Bismuth Eutectic (LBE), which gained interest in accelerator driven systems as a coolant and target. Without a protective oxide scale on metallic components, the dissolution rate will become unacceptably high.

The formation of an oxide scale leads to a local volume change, to a volume increase if the Pilling-Bedworth-Ratio is greater than one and to a decrease if it is smaller than one. Thus, large residual stresses can result from these volume changes, especially when the oxide scale forms on surfaces with large curvatures. Film cracking and/or spalling may be the consequence of these residual stresses. But even in case where they do not impair the mechanical integrity of the scale during steady-state operation, they may combine with stresses due to thermal cycling and lead then to detrimental effects.

There is still a considerable uncertainty about the stress distributions generated by oxidation, despite decades of study and debate. The oxidation stresses depend on the geometry of the metallic components and on the oxidation strain tensor. In case of a flat plate and under uniaxial oxidation normal to the surface of the plate, no oxidation stresses should develop, if the lateral surfaces of the plate are prevented from oxidizing. This is true for interface and surface oxidation conditions as well. If the oxidation strain tensor has lateral components, growth stresses will develop, which lead to a bending of the plate. This then constitutes a possibility to determine the lateral oxidation strain components. Dankov and Churaev [1] found that the oxidation of thin metallic layers produced stresses, which lead to the bending of the specimens. Rhines and Wolf [2] found evidence of lateral compressive growth stresses in oxide scales on Ni rods and axial length changes of up to 0.2%.

In tubes, the radius of curvature is not infinite as for flat plates and we obtain stresses due to geometrical effects also under uniaxial oxidation strain. The smaller the radius of curvature, the higher are the geometrical stress effects of oxidation.

There are a number of reviews on the modeling of stress generation due to oxide growth (e.g.[3-5]). But one can recognize that the problem of eventual lateral oxidation strain components has not received much attention, whereas more and more experimental results on residual stresses and their effects appear in the literature (e.g.[6-15]).

The consequences of geometrical effects on oxide scale integrity were extensively discussed by Manning [16]. He has defined a scale displacement vector, which mainly depends on the radius of curvature, the Pilling-Bedworth ratio, and the mode of oxidation (interface or surface oxidation). The displacement vector was derived more on intuitive arguments than on the principles of mechanics. Thus, it was concluded, that there is no growth stress in a duplex scale by simply adding the displacement vectors due to interface and surface oxidation. This procedure is at least doubtful. Also, the role of eventual lateral components in the oxidation strain tensor was not recognized.

Hsueh and Evans [17] developed a model for the residual stresses under cylindrical geometry based on the principles of mechanics considering also creep effects. They treated the cases of uniaxial and dilatational oxidation strain that means all three components of the oxidation strain tensor being equal. But this latter case seems rather unrealistic, as no oxide scale is known, which would behave in this manner. Also these authors didn't investigate the stress distributions in duplex scales, a case most relevant for steel components.

There are observations on length increases of austenitic steel tubes of about 2% caused by oxidation reported in the literature [10]. This gives us a clue on the magnitude of the axial oxidation strain component. Axial elongations were also reported in [11] for samples of Fe-Cr-Al-Y alloys with Al_2O_3 scales. Lateral oxide growth on 18Cr steel was also determined in [6] with values increasing with time up to about 3%. The formation of wrinkles on oxide scales on steels, for example, is attributed to lateral growth [18]. Hence, an effort to include lateral components of the oxidation strain tensor into the model is certainly warranted. It should also be noted that exact solutions of the stress-strain equations are of great value for the validation of numerical codes.

2. Development of the stress-strain model

The model is to be meant for the calculation of stress distributions in tubes. Therefore we take a cylindrical geometry as a basis. For other geometries like flat plates or spheres, the modifications which have to be applied, can easily be deduced. We assume that the oxide scales are formed at the outside of the tube. For oxide scales at the inside of the tube the part of the hoop stress which is due to the curvature of the tube would only change its sign. This would, of course, also affect the radial and axial stress components. It should be noted that we do not consider creep effects, neither in the metallic substrate nor in the oxide film.
We assume that we have, in general, a multi-axial oxidation strain tensor in the oxide film,

$$e^{ox} = (e_r^{ox}, e_\Theta^{ox}, e_z^{ox}) \tag{1}$$

with, in principle, different components in all three directions of space. Special cases like uniaxial oxidation strain with

$$e_r^{ox} = \Phi - 1 \qquad e_\Theta^{ox} = e_z^{ox} = 0 \tag{2}$$

and dilatational oxidation strain with

$$e_r^{ox} = e_\Theta^{ox} = e_z^{ox} = \Phi^{1/3} - 1 \tag{3}$$

were treated in [17]. But most interesting from a practical point of view seems to be an oxidation strain tensor with the main component being in radial direction and minor components in azimuthal and axial directions. The radial component of the oxidation strain tensor acts orthogonal to the interface between the oxide film and the metallic substrate and the other two components in parallel to the interface. Therefore we denote these as lateral components. Models for the calculation of growth strains in oxide scales on rods and tubes

have also been reported in refs. [19,20]. But it seems that these authors didn't recognize the importance of the oxidation mode (surface/interface oxidation).
There are indications from the literature [6], that the oxidation strain components may depend on the distance from the interface. But for this work we make the simplifying assumption that they are constant. The more general case can be treated with the help of a slight modification of some parameters. It should be noted, that we are using the non-displaced radii for the derivation of the solution and all locations in the oxide film are referred to the consumed metal layer.

Application of the generalized Hooke's law for the metallic substrate and the oxide film leads to the following stress-strain equations:

$$\begin{aligned} &E^s \cdot \varepsilon_i^s = \sigma_i^s - \nu^s \cdot (\sigma_j^s + \sigma_k^s) \\ &E^f (\varepsilon_i^f - e_i^{ox}) = \sigma_i^f - \nu^f \cdot (\sigma_j^f + \sigma_k^f) \\ &i, j, k = r, \Theta, z \end{aligned} \tag{4}$$

In each case three equations are established by cyclic permutation of i, j and k.
Symmetry about the z axis requires that the shear stress $\sigma_{r\Theta}$ be zero and that we have the following relations for equilibrium and compatibility:

$$\frac{d}{dr}\sigma_r = \frac{\sigma_\Theta - \sigma_r}{r} \tag{5}$$

$$\varepsilon_r = \frac{d}{dr}u \text{ and } \varepsilon_\Theta = \frac{u}{r} \tag{6}$$

where u denotes the radial displacement.

In general, we have to do with long cylinders. Hence, we can impose plane strain conditions for the metallic substrate and the oxide film. The treatment of end effects is outside the scope of this work.
The plane strain condition is applied in its generalized form:

$$\varepsilon_z = const. \tag{7}$$

as we foresee a non-zero axial component in the oxidation strain tensor. In case of uniaxial oxidation strain ($e^{ox}_z = 0$) we have found that the solutions lead to $\varepsilon_z \cong 0$ and we automatically fall back to the plane strain condition in its usual form. It should also be noted that axial strains upon oxidation of ferritic steel specimens are reported in the literature [18].
Using the compatibility relations (6), the stress-strain equations (4) and the condition of equilibrium (5), we can deduce the following differential equations for the radial stress in the oxide film:

$$(\frac{d}{dr}u^f - \frac{u^f}{r}) / r \quad = \quad (e_r^{ox} - e_\Theta^{ox}) / r - \frac{1+\nu^f}{E^f} \cdot \frac{d}{dr}\sigma_r^f \tag{8}$$

and using again the equilibrium condition and the stress-strain equations:

$$\frac{d}{dr}(\sigma_r^f + \sigma_\Theta^f) = \frac{E^f}{1-\nu_f^2} \cdot \frac{e_r^{ox} - e_\Theta^{ox}}{r} \tag{9}$$

We have assumed, that the components of the oxidation strain tensor do not depend on the radius r and we have made use of the plane strain condition. Otherwise we would have obtained derivatives of the lateral oxidation strain components and of the total axial strain of the oxide film.
The sum of the radial and hoop stress in the oxide film has the following dependence on the radius r:

$$\sigma_r^f(r) + \sigma_\Theta^f(r) = \frac{E^f \cdot (e_r^{ox} - e_\Theta^{ox})}{1-\nu_f^2} \cdot \ln(r / r_i^f) + C \tag{10}$$

where C being an integration constant.

Using again the condition of equilibrium in a cylinder (5) we obtain the following differential equation for the radial stress in the oxide film:

$$r \cdot \frac{d}{dr}\sigma_r^f + 2. \cdot \sigma_r^f = \frac{E^f \cdot (e_r^{ox} - e_\Theta^{ox})}{1-\nu_f^2} \cdot \ln(r / r_i^f) + C \tag{11}$$

Finally, we obtain the following solutions for the radial and hoop stresses in the oxide film:

$$\sigma_r^f(r) = \frac{B^f}{r^2} + D/2. \cdot \ln(r / r_i^f) - D/4. + C/2. \tag{12}$$

$$\sigma_\Theta^f(r) = -\frac{B^f}{r^2} + D/2. \cdot \ln(r / r_i^f) + D/4. + C/2. \tag{13}$$

The parameter D depends on the radial and azimuthal components of the oxidation strain tensor:

$$D = \frac{E^f}{1-\nu_f^2} \cdot (e_r^{ox} - e_\Theta^{ox}) \tag{14}$$

The parameters B^f and C can be determined with the help of the following boundary conditions:

$$\sigma_r^f(r_o^f) = 0 \quad \text{and} \quad \sigma_r^f(r_i^f) = \sigma_r^s(r_o^s) = \sigma_{r,\text{int}} \tag{15}$$

In this way, we have neglected an eventual coolant pressure at the outside of the tube, as this would have only a minor effect on the stress distributions.

$$B^f = \frac{{r_o^f}^2 \cdot {r_i^f}^2}{{r_o^f}^2 - {r_i^f}^2} \cdot (\sigma_{r,\text{int}} + D/2. \cdot \ln(r_o^f / r_i^f) \tag{16}$$

$$C = \frac{2 \cdot {r_i^f}^2}{{r_i^f}^2 - {r_o^f}^2} \cdot \sigma_{r,\mathrm{int}} + D/2. \cdot (1 + \frac{2{r_o^f}^2}{{r_i^f}^2 - {r_o^f}^2} \cdot \ln(r_o^f / r_i^f) \quad (17)$$

Thus, we have succeeded to express the radial and hoop stresses in the oxide film in terms of only two parameters, namely $\sigma_{r,int}$ and D.
From the condition of plane strain we can deduce that the axial stress in the oxide film must have the following form:

$$\sigma_z^f(r) = S_1 + \nu_f \cdot D \cdot \ln(r / r_i^f) \quad (18)$$

with S_1 being a constant. It should be noted that the axial stress in the oxide scale depends on the radius r.

For the metallic substrate we can make use of the Lame stress solutions for a cylinder:

$$\sigma_r^s(r) = A^s + \frac{B^s}{r^2} \quad (19)$$

$$\sigma_\Theta^s(r) = A^s - \frac{B^s}{r^2} \quad (20)$$

The parameters A^s and B^s can be determined with the help of the boundary conditions:

$$\sigma_r^s(r_i^s) = 0 \text{ and } \sigma_r^s(r_o^s) = \sigma_{r,\mathrm{int}} \quad (21)$$

$$B^s = \alpha \cdot \sigma_{r,\mathrm{int}} \text{ and } A^s = -\frac{\alpha}{{r_i^s}^2} \cdot \sigma_{r,\mathrm{int}} \quad (22)$$

$$\alpha = \frac{{r_i^s}^2 \cdot {r_o^s}^2}{{r_i^s}^2 - {r_o^s}^2} \quad (23)$$

As $\sigma_r^s + \sigma_\Theta^s$ is independent of r, the plane strain condition is fulfilled in the metallic substrate for:

$$\sigma_z^s = const. \quad (24)$$

The Lame solutions for the cylinder are derived under the assumption that the axial strain ε_z does not depend on the radius r, that is just the condition of generalized plane strain.
For a simple oxide scale we have now three unknowns, namely $\sigma_{r,\mathrm{int}}, S_1$ and σ_z^s, that means we need also three conditions for their determination. One condition is provided by:

$$\varepsilon_z^s(r_o^s) = \varepsilon_z^f(r_i^f) \quad (25)$$

Using Hooke's law and the stress solutions, which we have derived, we obtain the following equation:

$$\frac{\sigma_z^s}{E^s}+\frac{\nu_s}{E^s}\cdot\frac{2\alpha}{{r_i^s}^2}\sigma_{r,\mathrm{int}}=e_z^{ox}+\frac{S_1}{E^f}-\frac{\nu_f}{E^f}\cdot C \tag{26}$$

A further condition is provided by the axial force balance:

$$\int_{r_i^s}^{r_o^s} r\sigma_z^s dr+\int_{r_i^f}^{r_o^f} r(S_1+\nu_f\cdot D\cdot\ln(r/r_i^f))dr=0 \tag{27}$$

The last condition depends on the oxidation modus, that means whether the oxidation occurs at the interface due to anion transport or at the surface due to cation transport or at both locations like in a duplex scale.

2.1. Interface oxidation

In this case the third condition is given by:

$$u^s(r_o^s)=u^f(r_i^f) \tag{28}$$

which leads to the following equation:

$$\begin{aligned}&-\frac{\alpha}{E^s}(1/{r_i^s}^2+1/{r_o^s}^2)\sigma_{r,\mathrm{int}}-\frac{\nu_s}{E^s}(\sigma_{r,\mathrm{int}}+\sigma_z^s)=\\&e_\Theta^{ox}+(C-\sigma_{r,\mathrm{int}})/E^f-\frac{\nu_f}{E^f}(\sigma_{r,\mathrm{int}}+S_1)\end{aligned} \tag{29}$$

2.2. Surface oxidation

As in this case the cations are moving to the surface the consumed metal layer experiences a radial displacement. It is given by:

$$\Delta u^f=r_{d,i}^f-r_i^f \tag{30}$$

with the displaced inner radius of the consumed metal layer given as:

$$r_{d,i}^f=r_o^f-\frac{r_o^f-r_i^f}{e_r^{ox}+1} \tag{31}$$

Hence, we have the following condition:

$$u^s(r_o^s)=u^f(r_{d,i}^f)+\Delta u^f \tag{32}$$

This leads to an equation similar to (29) but with some modification on the right hand side.

$$\begin{aligned}&(-\frac{\alpha}{E^s}(1/{r_i^s}^2+1/{r_o^s}^2)\sigma_{r,\mathrm{int}}-\frac{\nu_s}{E^s}(\sigma_{r,\mathrm{int}}+\sigma_z^s))r_o^s=\\&\Delta u^f+r_{d,i}^f(e_\Theta^{ox}+(C-\sigma_{r,\mathrm{int}})/E^f-\frac{\nu_f}{E^f}(\sigma_{r,\mathrm{int}}+S_1))\end{aligned} \tag{33}$$

2.3. Duplex scale formation

We consider the case that we have interface oxidation in the inner subscale and surface oxidation in the outer subscale. Hence, we have a combination of both boundary conditions.
In each subscale we have a stress distribution like in (12) and (13), with, in general, different oxidation strain tensors in each subscale. We have in this case five unknowns, namely the radial interface stresses (metallic substrate/inner subscale and inner/outer subscale), which determine the distributions of the radial and hoop stresses, and the axial stresses in the three layers. We can establish five conditions in order to determine the five unknowns, namely the axial force balance, two conditions for the axial strain, and two conditions for the radial displacement at the two interfaces in each case.

$$u^s(r_o^s)=u^f(r_i^{f,i}) \tag{34}$$

and:

$$u^{f,i}(r_o^{f,i})=u^{f,o}(r_{d,i}^{f,o})+\Delta u^{f,o} \tag{35}$$

With the displaced inner radius of the outer subscale and the radial displacement given as:

$$r_{d,i}^{f,o}=r_o^{f,o}-(r_o^{f,o}-r_i^{f,i}-(e_r^{ox,i}+1)\cdot(r_o^{f,i}-r_i^{f,i}))/(e_r^{ox,o}+1) \tag{36}$$

$$\Delta u^{f,o}=r_{d,i}^{f,o}-r_o^{f,i} \tag{37}$$

Thus, we have established a system of linear equations for the determination of the unknowns (three unknowns for a simple scale and five unknowns for a duplex scale) of the form:

$$A\cdot\vec{x}=\vec{b} \tag{38}$$

The components of the matrix A and of the vector $\vec{b}$ depend on the dimensions of the metallic substrate and of the oxide film, on the mechanical properties of both phases, and on the oxidation strain tensor.

3. Creep in the metallic substrate

As the temperatures in the liquid metal loop of an ADS facility are foreseen to be distinctly below $T_m/2$ (with T_m being the melting temperature of the different materials) we do not expect creep effects in oxide scales, but there can be creep effects in the metallic substrate. In this case, the generalized Hooke's law in the metallic substrate is given as:

$$E^s \cdot (\varepsilon_i^s - \varepsilon_i^{cr,s}) = \sigma_i^s - \nu^s \cdot (\sigma_j^s + \sigma_k^s) \tag{39}$$

$\varepsilon_i^{cr,s}$: total creep strains in the metallic substrate

As the creep strains depend generally on the radial position, we can no longer apply the Lame solutions for the radial and hoop stresses, but we have now the following differential equation for the radial stress:

$$r \cdot \frac{d\sigma_r^s(r)}{dr} + 2 \cdot \sigma_r^s(r) = \frac{E^s}{1-\nu_s^2} \cdot \left(\int_{r_i^s}^{r} \frac{\varepsilon_r^{cr,s} - \varepsilon_\Theta^{cr,s}}{r} \cdot dr - \varepsilon_\Theta^{cr,s}(r) - \nu_s \cdot \varepsilon_z^{cr,s}(r) \right) + \hat{C}^s \tag{40}$$

with $\hat{C}^s$ as integration constant.

The integral in eq. (40) can, in general, not be solved analytically but only numerically.
The eq. (40) has the following solutions:

$$\begin{aligned} \sigma_r^s(r) = {} & \hat{C}^s/2 + \frac{B^s}{r^2} + \frac{E^s}{2(1-\nu_s^2)} \cdot \left(\int_{r_i^s}^{r} \frac{\varepsilon_r^{cr,s} - \varepsilon_\Theta^{cr,s}}{r} \cdot dr \right. \\ & \left. - \frac{1}{r^2} \cdot \int_{r_i^s}^{r} r \cdot ((\varepsilon_r^{cr,s} - \varepsilon_\Theta^{cr,s}) - 2 \cdot (\varepsilon_\Theta^{cr,s} + \nu_s \cdot \varepsilon_z^{cr,s}) \cdot dr) \right) \end{aligned} \tag{41}$$

$$\begin{aligned} \sigma_\Theta^s(r) = {} & \hat{C}^s/2 - \frac{B^s}{r^2} + \frac{E^s}{2 \cdot (1-\nu_s^2)} \cdot \left(\int_{r_i^s}^{r} \frac{\varepsilon_r^{cr,s} - \varepsilon_\Theta^{cr,s}}{r} \cdot dr \right. \\ & \left. + \frac{1}{r^2} \int_{r_i^s}^{r} r \cdot ((\varepsilon_r^{cr,s} - \varepsilon_\Theta^{cr,s}) - 2. \cdot (\varepsilon_\Theta^{cr,s} + \nu_s \varepsilon_z^{cr,s})) \cdot dr - (\varepsilon_\Theta^{cr,s}(r) + \nu_s \cdot \varepsilon_z^{cr,s}(r)) \right) \end{aligned} \tag{42}$$

With the help of the condition of generalized plain strain we can deduce, that the axial stress in the metallic substrate must have the following form:

$$\sigma_z^s(r) = S_0 + \frac{\nu_s \cdot E^s}{(1-\nu_s^2)} \cdot \left(\int_{r_i^s}^{r} \frac{\varepsilon_r^{cr,s} - \varepsilon_\Theta^{cr,s}}{r} \cdot dr - \varepsilon_\Theta^{cr,s} - \nu_s \cdot \varepsilon_z^{cr,s} \right) - E^s \cdot \varepsilon_z^{cr,s} \tag{43}$$

The parameters S_0, B^s, and $\hat{C}^s$ can be determined with the help of the boundary conditions in the same way as demonstrated in the previous section.

As the stresses in general change with time the total creep strains are calculated via the accumulation of creep strain increments:

$$\varepsilon_i^{cr,s} = \sum_{\Delta t_n} \Delta\varepsilon_i^{cr,s} \tag{44}$$

The creep increments within a time interval Δt are calculated with the help of the Prandl-Reuss flow rules:

$$\begin{aligned} \Delta\varepsilon_i^{cr,s} &= \frac{3}{2} \cdot \frac{s_i}{\sigma_{eq}} \cdot \Delta\varepsilon_{eq}^{cr} \\ s_i &= \sigma_i^s - 1/3 \cdot (\sigma_i^s + \sigma_j^s + \sigma_k^s) \end{aligned} \tag{45}$$

The equivalent stress σ_{eq} is given by von Mises as:

$$\sigma_{eq} = \sqrt{((\sigma_r^s - \sigma_\Theta^s)^2 + (\sigma_r^s - \sigma_z^s)^2 + (\sigma_\Theta^s - \sigma_z^s)^2)/2} \tag{46}$$

The secondary creep rates of metals are generally given in the following form:

$$\dot{\varepsilon}^{cr} = c \cdot \sigma^n \cdot e^{-Q/T} \tag{47}$$

c : constant
Q : activation energy

The equivalent creep increment in a time interval Δt is then given as:

$$\Delta\varepsilon_{eq}^{cr} = \dot{\varepsilon}(\sigma_{eq}, T) \cdot \Delta t \tag{48}$$

The length of the time interval Δt is to be chosen in such a way, that the stresses are fairly constant during that time interval.

4. Thermal cycling

If one wants to calculate the combined effect of oxidation and temperature changes, one has to use the generalized Hooke's in the following form:

$$E^f \cdot (\varepsilon_i^f - e_i^{ox} - \alpha^f \cdot \Delta T) = \sigma_i^f - \nu_f \cdot (\sigma_j^f + \sigma_k^f) \tag{49}$$

$$E^s \cdot (\varepsilon_i^s - \alpha^s \cdot \Delta T) = \sigma_i^s - \nu_s \cdot (\sigma_j^s + \sigma_k^s) \tag{50}$$

We do only consider situations, where the temperature is uniform over the tube. We also assume that the thermal expansion in the metallic substrate and in the oxide film is isotropic. Under these premises we can apply the procedure of section , as we have no logarithmic term in the stress distributions of the metallic substrate and can therefore use the Lame solutions. We have only to do the following transformations in the coefficients for the determination of the unknowns:

$$e_i^{ox} \rightarrow e_i^{ox} + (\alpha^f - \alpha^s) \cdot \Delta T \tag{51}$$

The stresses arising from temperature changes can also be estimated with the help of the following formula:

$$\sigma_{\Theta}^{f,th.} = \sigma_z^{f,th.} = \int_{T_i}^{T_e} \Delta\alpha \cdot \frac{E_f}{1-\nu_f} \cdot \frac{1}{1+\frac{1-\nu_{me}}{1-\nu_f} \cdot \frac{E_f \cdot \delta_{ox}}{E_{me} \cdot s_{me}}} \cdot dT \tag{52}$$

$\Delta\alpha = \alpha_f - \alpha_{me}$
T_i : initial temperature T_e : end temperature of the ramp

The importance of the thermal expansion coefficients α_f and α_m in the oxide scale and in the metallic substrate is obvious from eq. (52). If $\Delta\alpha$ is negative we will obtain tensile stresses in a downwards temperature ramp, if it is positive we will obtain compressive stresses.

If we have a duplex scale the thermal stresses in each subscale can also be calculated with the help of eq. (52), one has to use in this case for each subscale the appropriate thermal expansion coefficient for the oxide material.

5. Results of the sensivity studies on the consequences of lateral oxidation strains

For the parametric studies we have deliberately omitted relaxation mechanisms, as our main aim was to discern the effect of lateral oxidation strains. Including creep or other relaxation mechanisms may eventually partially obscure the results.

We are mainly interested in the case of oxide scales on stainless steel tubes under the conditions of e.g. an accelerator driven system. Depending on the temperature and the oxygen content in the liquid metal Fe/Cr spinel scales or magnetite/spinel duplex scales can be formed. The sensitivity studies were mainly meant for this situation. For the sake of completeness we have also considered the case of a single scale with surface oxidation. The data, which were used for the calculations are listed in Tab. 1.

Table 1 : Input data for the sensitivity studies

Outer tube diameter	8 mm	Young's modulus E^{me}	1.6 10^5 MPa
Inner tube diameter	6 mm	Young's modulus E^{ox}	1.8 10^5 MPa
Pilling Bedworth ratio Φ	2.0	Poisson ratio ν^{me}	0.3
Consumed metal layer (standard case)	10 µm	Poisson ratio ν^{ox}	0.29

The same value for the radius of curvature of the tubes has been used in all the calculations. For the oxidation strain tensor we made the assumption, that the axial and azimuthal components are equal and as the lateral components are rather small compared to the radial one, we can use the following approximation:

$$\Phi - 1 \quad = \quad \sum_i e_i^{ox} \tag{53}$$

It should be noted that we assume, that the oxide films are formed on the outer (convex) surface of the tubes. If the oxidation would occur at the inner (concave) side of the tube, we would obtain a reversal of the stress state in case of uniaxial oxidation strain. In case of multi-axial oxidation strain only that part of the stress, which is due to curvature of the metallic substrate would reverse its sign.
The mechanical data (taken from [21-22]) are for austenitic steels at 550°C, a typical temperature in LBE loops.

For uniaxial oxidation strain one has tensile hoop and axial stresses in the oxide scale in case of interface oxidation and compressive stresses of about the same absolute value in case of surface oxidation (see Figs. 1-2). This is in accordance with results in [16,17].

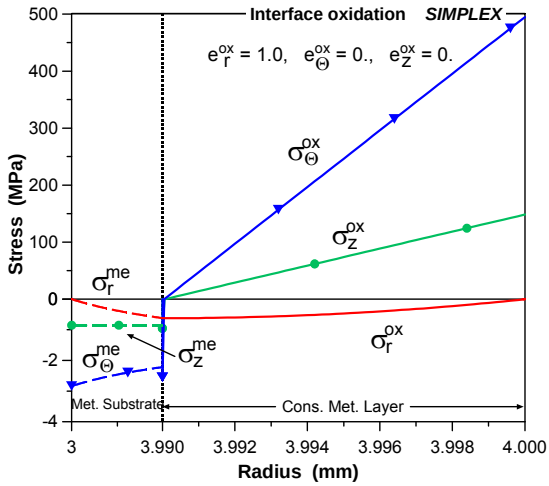

Fig. 1 : Stress distribution in the tube under uniaxial oxidation strain (**interface oxidation**).

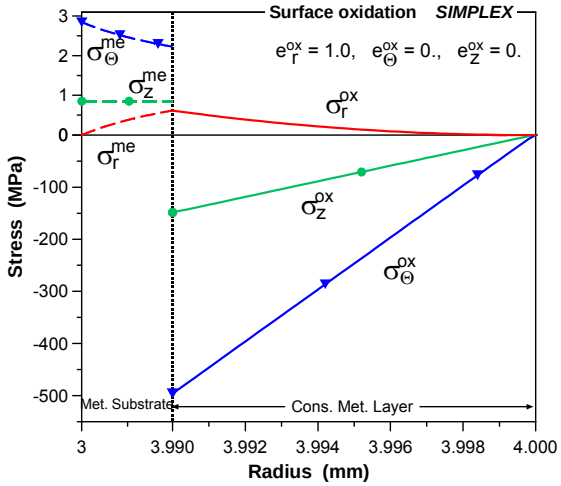

Fig. 2 : Stress distribution in the tube under uniaxial oxidation strain (**surface oxidation**).

Based on the work of Manning [16] we have derived the following formula for the maximum hoop stress in the oxide film under interface oxidation [23]:

$$\sigma_{\Theta}^{f,\max} = (\Phi - 1) \cdot \frac{h}{r_0^f} \cdot \frac{E_f}{1 + \frac{E_f}{E_{me}} \cdot \frac{\Phi \cdot h}{s_{me}}} \qquad (54)$$

where h is the consumed metal layer and s^{me} the remaining metal layer in the tube (e.g. clad) wall.

For the hoop stress at the interface we obtain with the data given in Tab. 1 a value of 440 MPa and assuming surface oxidation a value of -440 MPa. The values of our analytical solution differ about 10%.

In case of a duplex scale, we have tensile stresses in the inner subscale, where interface oxidation occurs, and correspondingly compressive stresses in the outer subscale (see Fig.3). The mean hoop stress in the symmetric duplex scale is roughly zero, and only in this sense the simple model of Manning [16] would give a correct prediction. But, of course, the knowledge of the mean hoop stress in a duplex scale is certainly not sufficient for an assessment of the stress situation. For an asymmetric duplex scale we have a non-zero mean hoop stress (see Fig.4) showing again the limitations of the Manning's model. The strain in the oxide film is in this model determined by a displacement vector and this vector was defined as zero in case of a duplex scale (see Table 2 in ref. [16]). But this can at best be correct in case of a symmetric duplex scale. For an asymmetric duplex scale a weighed average procedure should be applied.

There is a discontinuity in the hoop and axial stresses at the interface of the two sublayers. This is a consequence of the mixed mode of the oxidation. In the inner sublayer we have tensile hoop and axial stresses due to the interface oxidation mode and in the outer sublayer compressive stresses due to the surface oxidation mode.

A discontinuity in the hoop and axial stresses is not an unusual feature. For a hollow cylinder there is, for example, in any case a discontinuity at the interface of the oxide scale and the metallic substrate. Only the radial stress must under all circumstances be continuous. This is a consequence of the equilibrium condition. It can be taken from Figs. 1-4 that our solutions fulfill the requirement of a continuous radial stress.

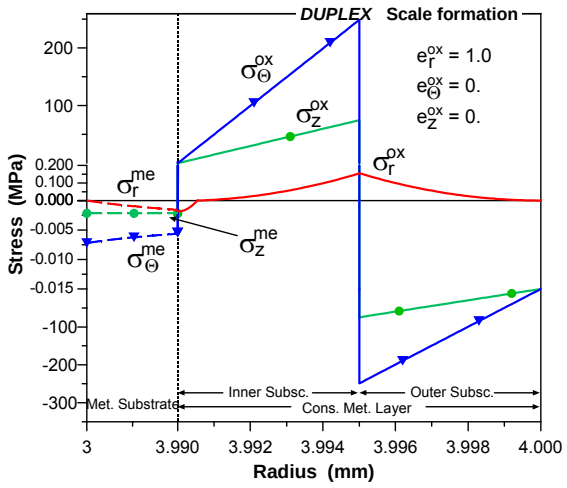

Fig. 3 : Stress distribution in the tube under uniaxial oxidation strain (**symmetric duplex** scale).

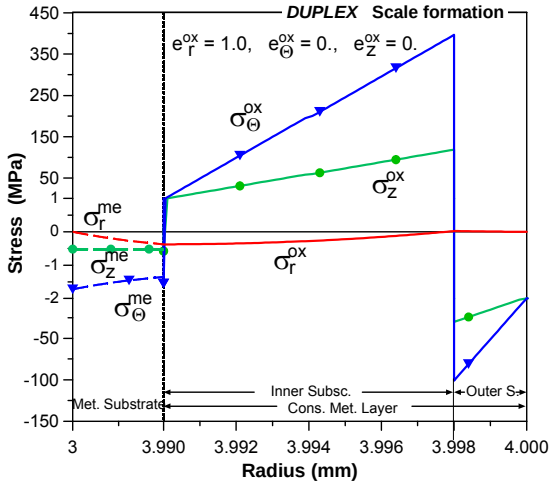

Fig. 4 : Stress distribution in the tube under uniaxial oxidation strain (**asymmetric duplex** scale)

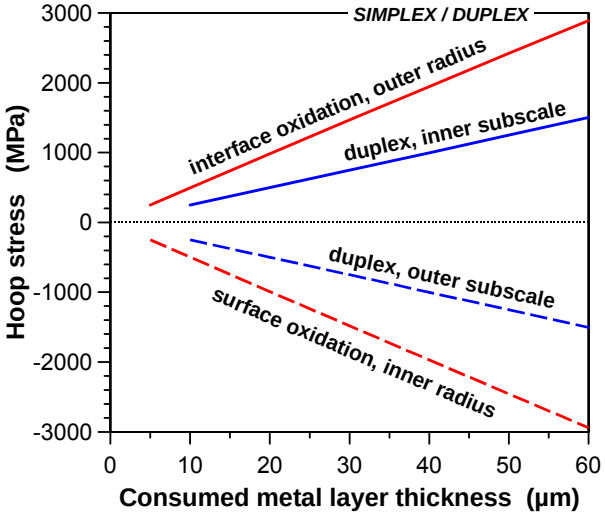

Fig. 5 : Hoop stress versus consumed metal layer thickness for uniaxial oxidation strain.

For a consumed metal layer of 10 µm, that means an oxide scale thickness of 20 µm, we have maximum absolute hoop stress values of about 500 MPa for the simple scale and about 250 MPa for the symmetric duplex scale. It should also be noted that as a general rule the oldest oxide is in the highest stress state. The maximum hoop stress increases linearly with the thickness of the consumed metal layer (see Fig.5). This feature confirms also the simple model of Manning [16].

All the results presented so far were for uniaxial oxidation strain. In the following we are going to investigate the consequences of lateral components of the oxidation strain tensor. For the sake of simplicity we assume that the azimuthal and axial components are equal. It is also assumed that these lateral components (azimuthal/axial) are small compared to the radial one, as this seems most relevant for practical applications of the model. But the model is, of course, apt to treat also other conditions. We also assume that the oxidation strain tensor is the same in both subscales of the duplex scale. In the following we are going to discuss the results of sensitivity studies concerning the effects of eventual lateral components in the oxidation strain tensor.

Lateral components of the oxidation strain may have a considerable effect, as can be taken from Figs. 6-8. Even for lateral components as small as 0.005 the hoop stress becomes

distinctly compressive in case of surface oxidation and the axial stress is in all cases comparable to the hoop stress. This is a consequence of our assumption that the axial and azimuthal components of the oxidation strain tensor are equal. The whole duplex scale is now clearly in a compressive stress state. In any case the simple model of Manning is in this case inadequate as it considers only the geometrically induced growth stresses. The difference between inner and outer hoop stress in the oxide film is due to the radial oxidation strain component. It is comparable in magnitude to that for the uniaxial case, as the radial component does not change very much.

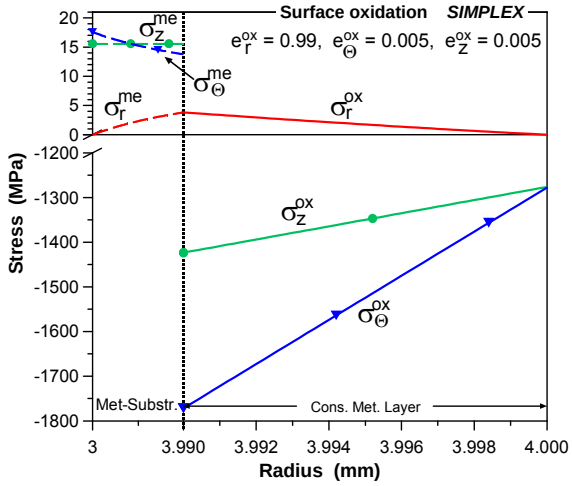

Fig. 6 : Stress distribution in the tube under multi-axial oxidation strain (**surface oxidation**).

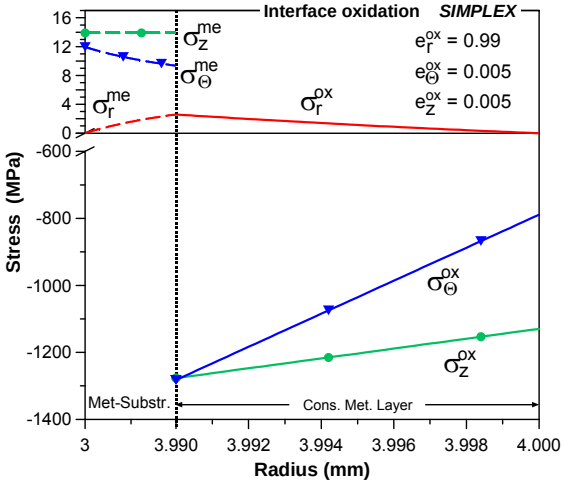

Fig. 7 : Stress distribution in the tube under multi-axial oxidation strain (**interface oxidation**).

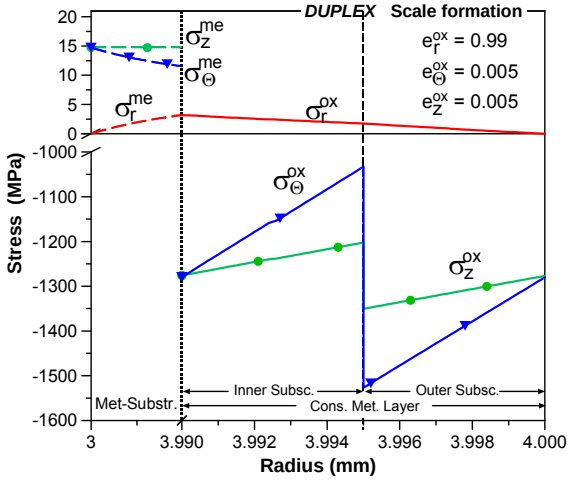

Fig. 8 : Stress distribution in the tube under multi-axial oxidation strain (**symmetric duplex** scale).

It should be noted that the stress is now roughly the same in all three cases of the oxidation mode (surface, interface oxidation, and duplex scale formation), although there are still some differences in the stress distributions. The stress situation is largely determined by the lateral components, the absolute stress level being roughly an order of magnitude higher than for uniaxial oxidation strain for a value of 0.02 for the lateral oxidation strain components. This is rather astonishing as the lateral fraction of the volume increase comprises only 4%.

The hoop stresses at the outer (interface oxidation) and inner (surface oxidation) scale radius respectively at the interface of the two subscales (duplex scale formation) are plotted in Fig.9 versus the lateral oxidation strain.

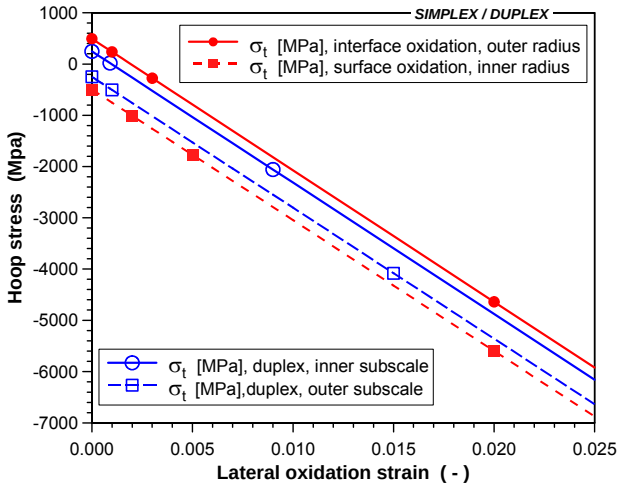

Fig. 9 : Hoop stress versus lateral oxidation strain.

The hoop stresses vary linearly with the lateral oxidation strain. For interface oxidation the change from a tensile to a compressive stress situation occurs at a lateral oxidation strain of only 0.002. For thicker oxide scales or thinner tubes correspondingly higher lateral oxidation strains would be needed to achieve the same effect. The stress values under three-dimensional oxidation strain converge to that for the uniaxial case for $e_\Theta^{ox} = e_z^{ox} \rightarrow 0$. This gives us confidence, that the solutions for the multi-dimensional case are correct.

In the literature on growth stresses it is often distinguished between geometrically induced growth stresses and intrinsic growth stresses (see for example ref. [6]). In the light of our model we can state, that the geometrically induced contribution is caused by the oxidation strain component which acts orthogonal to the surface and the intrinsic contribution is caused by the lateral strain components. To the knowledge of the authors this viewpoint has never been expressed in such a clear way. It should also be mentioned that the growth stresses in ref. [16] refer only the geometrically induced part. Geometrically induced growth stresses do only appear in specimens with a finite radius of curvature, as is evident from eq. (54).

We consider a dilatational volume increase upon oxidation as rather unrealistic. Nevertheless, it is of some interest to estimate the stresses in the oxide film, which we would obtain in this case. We have derived the following approximate formula for the case of dilatational oxidation strain:

$$\sigma_\Theta^f = \sigma_z^f = -(\Phi^{1/3} - 1) \cdot \frac{E_f}{1-\nu_f} \cdot \frac{1}{1 + \frac{h \cdot \Phi}{s_{me}} \cdot \frac{1-\nu_{me}}{1-\nu_f} \frac{E_f}{E_{me}}} \qquad (55)$$

With the data in Tab. 1 we obtain the following estimation of stress values in the oxide film:

$$\sigma_\Theta^f = \sigma_z^f = -0.37 \cdot E^f = -6.6 \cdot 10^4 \, MPa \qquad (56)$$

That is one order of magnitude greater than the stress values for a lateral oxidation strain of 0.02. As under dilatational volume increase the linear oxidation strain is about 0.26, the stresses for both cases have roughly the same ratio as the oxidation strains. These stress values for the case of isotropic expansion are of course very high and rather unrealistic. The

main aim for the sensitivity studies was to demonstrate the effect of lateral components in the oxidation strain tensor. But one should not forget that there is a volume increase of 100% upon oxidation. For a comparison one may also note that in metal alloys the elastic limit is reached at a tensile strain of less than 0.2%. Also, our model is purely elastic. With inelastic processes like creep, plastic flow, or micro-cracking the stresses in the oxide film could be reduced considerably.

In case of a short annular cylinder we can apply the plane stress condition ($\sigma_z = 0$) and obtain the following formula for the hoop stress in the oxide scale under isotropic expansion:

$$\sigma_{\Theta}^{f} = -(\Phi^{1/3} - 1) \cdot \frac{E_f}{1 + \frac{E_f}{E_{me}} \cdot \frac{h \cdot \Phi}{s_{me}}} \tag{57}$$

Hence, the difference in hoop stresses between the two limiting approximations of plane strain and plane stress is determined by the factors 1/(1-ν) and 1. We have essentially a bi-axial stress state in case of plane strain and in case of plane stress essentially a uniaxial stress state. The radial stress is in both cases small compared to the hoop stress. The formulas (55) and (57) can be extrapolated to the non-isotropic expansion in case that both lateral strain components (azimuthal and axial) are equal. Replacing ($\Phi^{1/3} - 1$) by e_{Θ}^{ox} in (55) and (57) we obtain approximate expressions for the intrinsic hoop stresses in the oxide scale:

$$\sigma_{\Theta}^{\text{intr.gr.}} = -e_{\Theta}^{ox} \cdot \frac{E_f}{1 - \nu_f} \cdot \frac{1}{1 + \frac{h \cdot \Phi}{s_{me}} \cdot \frac{1 - \nu_{me}}{1 - \nu_f} \frac{E_f}{E_{me}}} \tag{58}$$

Fig.10 shows the total axial elongation versus the oxide scale thickness for two values of the lateral oxidation strain. We recognize that the total axial strain increases linearly with the oxide scale thickness and with the lateral oxidation strain. By using the condition of generalized plane strain we may have a chance to reproduce measured axial expansions upon oxidation. In order to achieve this aim, some improvement of the model is needed with the implementation of stress relief mechanisms.

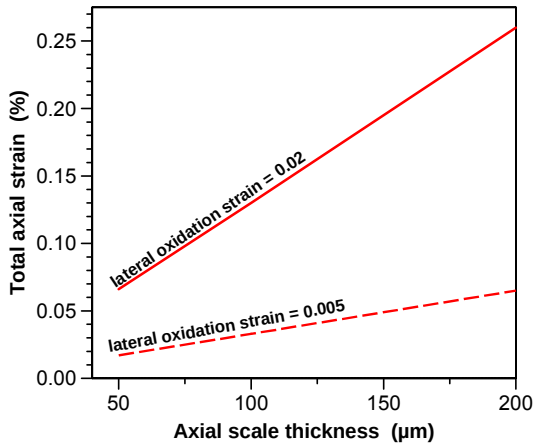

Fig. 10: Total axial strain versus oxide scale thickness with the lateral oxidation strain as a parameter.

6. Results of calculations for stresses in duplex scales on stainless steel tubes due to oxidation and thermal cycling

The stresses due to thermal cycling in single layer scales are generally calculated with the help of relatively simple formula (see for example ref. [24]. This procedure has been generalized to duplex scales in ref. [25]. In this reference also the superposition of stresses due to oxidation and thermal cycling was treated in a similar way. The newly developed model offers now the possibility to deal with this problem in a more rigorous manner. The data for the calculations, whose results are to be discussed in the following, were taken from refs. [26-30]. For further information on these data the reader is referred to ref. [25]. The mechanical data for magnetite and Fe/Cr spinel used for the calculations are listed in Tab. 2 also taken from ref. [25].

Table 2 : Summary of mechanical properties used for the calculations of temperature ramps.

	Fe_3O_4	$FeCr_2O_4$
Young's modulus E_{ox} in MPa	$2.1\ 10^5$	$2.33\ 10^5$
Poisson ratio ν	0.29	0.31
Surface fracture energy γ_s in J/m^2	4.5	5.0
Fracture toughness K_{Ic} in $MPa*m^{1/2}$	1.4	1.5
$\gamma_s \cdot E_{ox}$ in $MPa^2 \cdot mm$	945	1165
Pilling-Bedworth ratio Φ	2.07	2.07

The calculations discussed in ref. [25] were for austenitic, martensitic and ferritic steels as there is an interesting difference in the thermal expansion coefficient among them. In this report we consider only austenitic steels, as the aim of this chapter is to demonstrate the capabilities of the model. Three cases have been studied, namely the stress distribution in the duplex scale due to oxidation alone (Fig.11, $e_{lat}^{ox} = 0$) and the combined effect of growth stresses and thermal cycling stresses (Fig.12 and 13, ΔT = -600 K) with and without lateral oxidation strains ($e_{lat}^{ox} = 0$; $e_{lat}^{ox} = 0.005$). We have taken the same value of the lateral oxidation strain in both subscales.

With the simple formula for geometrically induced growth stresses we would obtain for the maximum hoop stress in the Fe/Cr spinel subscale a value of 599 MPa and in the magnetite subscale a value of -543 MPa. The values of the analytical model are about 10 % higher in absolute value. This is probably due to the fact that the effect of axial stress is disregarded in the approximate formula.

For a temperature ramp of -600 K one would obtain with the approximate formula of ref. [25] for the change of the mean hoop stress in the Fe/Cr subscale a value of about -840 MPa and in the magnetite subscale a value of about -480 MPa. Doing the superposition of both stress

effects with the help of the approximate formula one would arrive for the mean hoop stress in the inner subscale at about -540 MPa and in the outer scale at about -750 MPa. As can be taken from Fig.12, the analytical model yields mean values of about -400 MPa and of about -680 MPa. Thus, there is a difference of 10 - 25 %.

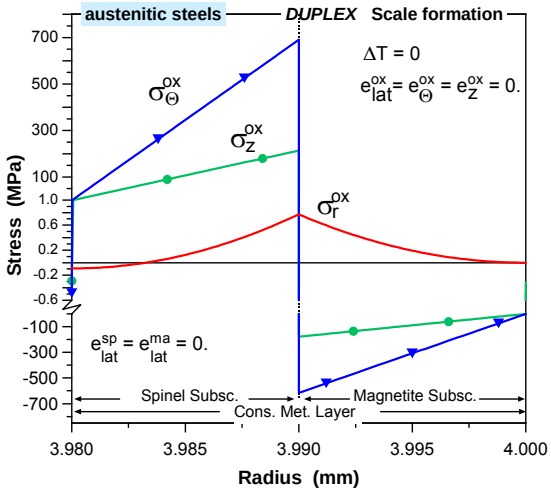

Fig. 11: Distribution of growth stresses in a duplex scale on austenitic steels (scale thickness 40 µm, e^{ox}_{lat}=0.)

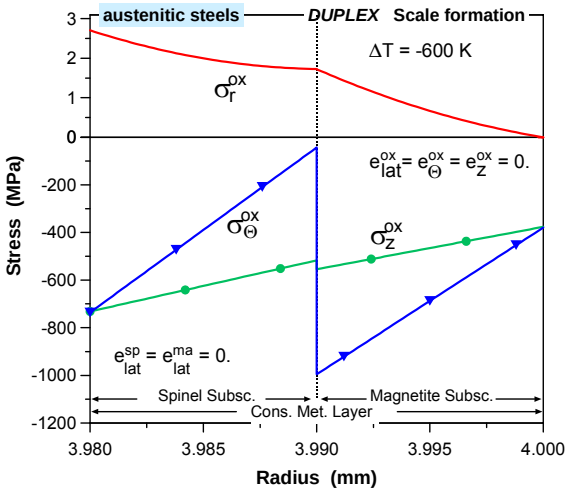

Fig. 12: Distribution of stresses in a duplex scale on austenitic steels after growth and a temperature ramp of -600 K (scale thickness 40 µm)

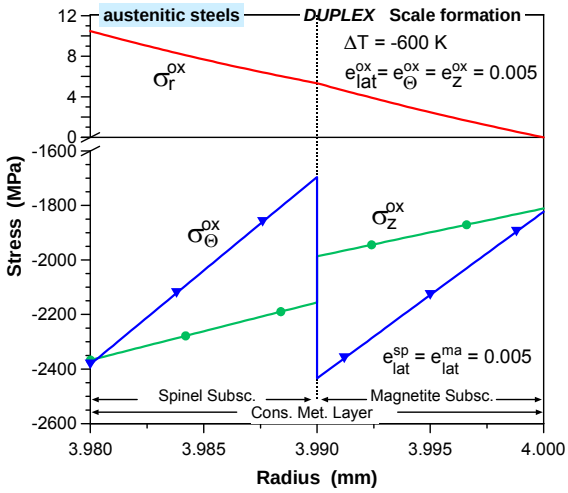

Fig. 13: Distribution of stresses in a duplex scale on austenitic steels after growth and a temperature ramp of -600 K (scale thickness 40 µm, e^{ox}_{lat}=0.005)

With a lateral oxidation strain of 0.005 we would obtain with the data in Tab. 2 and using formula (58) the following values for the mean intrinsic growth stresses:

$$\sigma_{\Theta}^{intr,sp} = \text{-1688 MPa} \qquad \sigma_{\Theta}^{intr,ma} = \quad \text{-1479 MPa}$$

Superposition with the stresses due to the downwards temperature ramp would yield at the end of the temperature ramp mean hoop stress values of -2520 MPa and -1959 MPa in the inner and outer subscale. These values are to be compared to that of the analytical model with a mean hoop stress in the inner subscale of about -2000 MPa and of about -2100 MPa in the outer subscale. Taking into account the geometrically induced growth stresses would improve the situation for the approximate formulas considerably as this effect gives a tensile contribution (300 MPa) in the inner subscale and a compressive one (-271 MPa) in the outer subscale.

7. Dimensional changes during Zry oxidation in air atmosphere

The most intriguing feature observed during the scaling of Zr in air is its dimensional instability [31]. The increase in lateral dimensions is permanent and of large magnitude due to the joint presence of oxygen and nitrogen. It was remarked in [31] that this effect is due to growth stresses, but the importance of lateral oxidation strains was not recognized. It should be noted that the results of ref. [31] indicate that there is symmetry in the two lateral directions.

Isothermal oxidation tests in air atmosphere with tube sections of Zry (outer diameter 10.75 mm, wall thickness 0.725 mm) have also been done at FZK/IMF [32] with temperatures between 800 and 1100ºC. The measured values of outer diameter increase were used as a basis for comparison with a simplified version of our model. Unfortunately, no values of the axial extensions of the test specimens were given in ref. [32].

In the temperature range investigated in refs. [31,32] occurs break-away oxidation after some incubation period due to cracking in the oxide scale. Thus, to a first approximation the growth of the scale can be described with the help of the following time law:

$$\frac{d}{dt}\delta_{ox}(t) = \frac{k^{par}}{\delta_{ox}} \quad \text{for} \quad f \le 1 \tag{59}$$

$$\frac{d}{dt}\delta_{ox}(t) = a^{lin} \quad \text{for} \quad f > 1 \tag{60}$$

a^{lin} : linear rate parameter
k^{par} : parabolic rate constant

In this way we have neglected the transition phase ranging between that of parabolic growth and the regime of linear growth.
The failure parameter f is determined with the help of a life fraction rule:

$$f(t) = \sum_i \frac{\Delta t_i}{t_f(T)} \qquad (61)$$

t_f = time to reach beak-away regime

The summation in eq. (61) goes over all Δt_i up to a certain time t. With this formulation of the model we can also treat transient conditions.

In a first step we have done scoping calculations with our novel solution technique for the creep problem during the parabolic oxidation phase assuming only outside tube oxidation. (The simulation of outside and inside tube oxidation is not yet possible with our new model.) A lateral oxidation strain of 0.005 was assumed. Correlations for creep of β-Zry and of α-Zr(O) have been taken from refs. [33,34]. The action of creep of the metallic substrate is at best exemplified by the evolution of the mean hoop stress in the scale. This is shown in Fig.14 for the temperatures of 800 and 1000ºC. As the metallic substrate creeps against the scale it exerts a tensile stress on it, relieving the compressive stress in the scale to some extent. At 800ºC the stress relaxation effect is only moderate over a test duration of more than 7000 s (about 20%), but at 1000ºC there is a considerable relaxation effect (about 90% in 900 s).

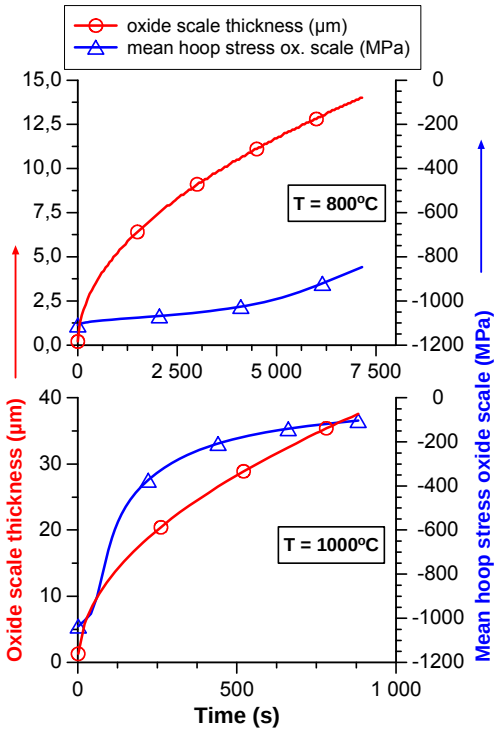

Fig. 14: Evolution of the mean hoop stress in the scale on Zry tube sections and scale thickness (parabolic regime, e^{ox}_{lat} = 0.005).

The mechanical behavior is characterized by a series of cracking processes and we hold that the sound scale oscillates around a time averaged value given by:

$$\delta_{ox}^{av,s} = 1/2 \cdot \frac{k^{par}}{a^{lin}} \qquad (62)$$

Due to the experience gained in ref. [31] we can assume a bi-axial stress state in the sound oxide scale and in the metallic substrate. We can surmise that the intrinsic growth stresses in the oxide scale are largely dominating the geometrically induced growth stresses. As the new oxide grows at the interface with the metallic substrate, as oxygen and nitrogen are diffusing through the scale, we have tensile geometrically induced growth stresses. For an oxide scale of 5 µm, for example, the maximum value for the geometrically induced hoop stress would be 40 MPa. Thus, geometrically induced growth stresses can not explain the observed dimensional changes of the tube sections.

Due to the rather large uncertainties of the scale formation in the break-away regime (cracking is essentially a stochastic process) and due to some deficiencies of the standard model it deemed us necessary to develop a simplified model. In this model the following expression for the intrinsic growth stress in the scale is used:

$$\sigma_{\Theta}^{ox} = \frac{-E_{ox}}{1-\nu_{ox}} \cdot e_{lat}^{ox} \tag{63}$$

The main assumption is that the growth stresses in the scale do not change with time.
The hoop stress in the metallic substrate can be calculated with the help of the force balance (there is inside and outside oxidation of the tube sections):

$$2 \cdot \delta_{ox}^{av,s} \cdot \sigma_{\Theta}^{ox} + s_{me} \cdot \sigma_{\Theta}^{me} = 0 \tag{64}$$

For the calculation of creep in the metallic substrate we use the correlation given by Burton [33] for the secondary creep rate of Zircaloy-4:

$$\dot{\varepsilon}^{cr} = 1.83 \cdot 10^{17} \cdot (G/T) \cdot (\sigma/G)^{5.32} \cdot e^{-3.27 \cdot 10^4 / T} \tag{65}$$

where the shear modulus G is given by:

$$G = 3.326 \cdot 10^{10} - 2.244 \cdot 10^{7} \cdot (T-273) + 2.161 \cdot 10^{3} \cdot (T-273)^2 \tag{66}$$

G, σ in N/m^2 and $\dot{\varepsilon}$ in 1/s

Using the flow rules of Prandl-Reuss and the equivalent stress according to von Mises we obtain for the creep increment in azimuthal direction in a time interval Δt:

$$\Delta\varepsilon_{\Theta}^{me,cr} = 1/2 \cdot \Delta\varepsilon_{eq}^{me,cr} = 1/2 \cdot \Delta t \cdot \dot{\varepsilon}^{cr}(T, \sigma_{eq}^{me}) \tag{67}$$

The increase of the outer radius in a time interval Δt is the given by:

$$\Delta r_{cl,o} = r_{me,av} \cdot \Delta\varepsilon_{\Theta}^{me,cr} + \Delta\delta_{ox}(1 - 1/\Phi) \tag{68}$$

ZrO_2: Φ= 1.56; ZrN: Φ= 1.06

and the change of the metallic substrate thickness:

$$\Delta s_{me} = -2 \cdot \Delta\delta_{ox} / \Phi \tag{69}$$

We have calculated with this simple model as described above the outer diameter increase of the tube sections during the break-away phase for three temperatures (800, 900 and 1000ºC) and made the comparison with the values measured at FZK/IMF. The results are to be seen in Fig.15. At 800 and 900ºC the evolution of the measured diameter increase is relatively well matched by the calculation. There is a problem with the transition phase and

the beginning of the proper break-away regime, and we have also not understood why in the parabolic phase the measured diameter increase is considerably higher than expected by the volume increase due to oxidation.

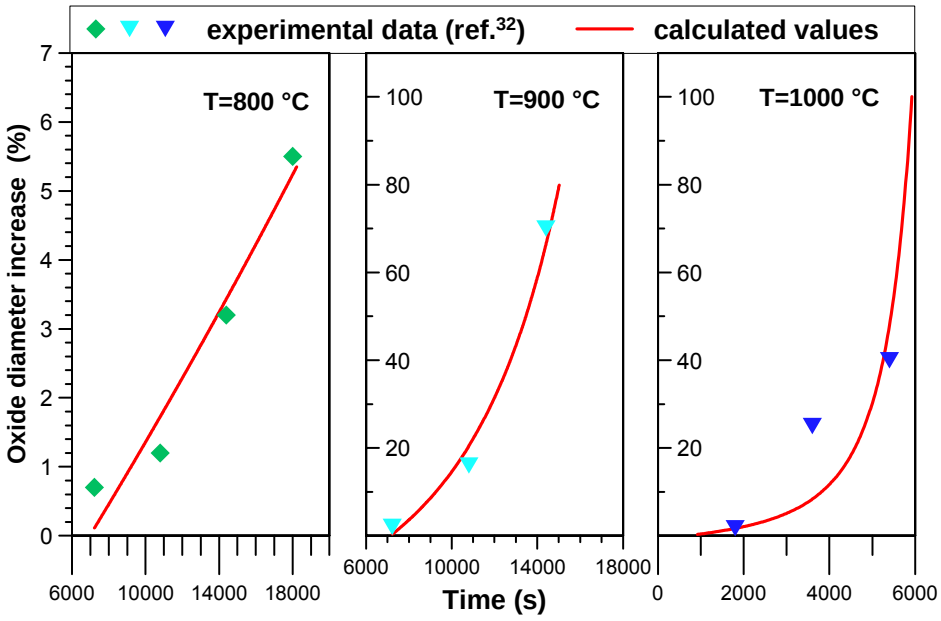

Fig. 15: Outer diameter increase of Zry tube sections in air: comparison of calculated and measured values.

The agreement is not so good at 1000ºC. We think that this is presumably due to the assumption of constant growth stresses in the scale, which is not fulfilled in this case. Values of some characteristic input and output data of the calculations are to be found in Tab. 3. Values for the lateral oxidation strain, for example, range between 0.00075 and 0.0025 and the hoop stress in the sound oxide scales between -248 and -704 MPa. Thus, our assumption on the importance of geometrically induced growth stresses seems well justified. It should be noted, that the mechanical behavior of the metal oxide system during Zr alloy oxidation was also modeled in ref. [35] assuming lateral oxidation strains of 0.005 for each lateral direction.

Table 3 : Input and output data for Zry oxidation under air atmosphere.

T (ºC)	a^{lin} (cm/s)	e_{lat}^{ox}	$\delta_{ox}^{av,s}$ (µm)	σ_{Θ}^{av} (MPa)
800	$1.\ 10^{-7}$	0.002	6.9	-704
900	$1.39\ 10^{-6}$	0.0025	4.5	-853
1000	$6.\ 10^{-6}$	0.00075	6.7	-248

8. Discussion of experimental data found in the literature

The newly developed model allows the calculation of growth stresses in oxidizing tubes under uniaxial and multi-axial oxidation strain tensors. The occurrence of lateral components may have a marked effect on the stress situation in the composite. The consequences of the stresses can eventually be studied by the mechanical effects on the oxide film itself or by the dimensional changes of the composite or both. Tensile stresses can lead to tensile cracks and compressive stresses to shear cracks and eventually to spalling and decohesion effects. The oxidation of Zircaloy, for example, is determined by oxygen transport and the oxidation is therefore clearly of the interface type. If the oxidation strain tensor of this material is uniaxial, we would expect the formation of tensile cracks beginning at the surface of the scale and propagating further into it in the course of time. But the actual crack configuration is clearly different [36]. In the so-called break-away regime, numerous shear cracks are observed in the interior of the oxide scale. This indicates that there is a compressive stress state in the scale. By a precise dimensional control of oxidizing Zircaloy tubes we could obtain information on the lateral components of the oxidation strain tensor, which seems indispensable for a mechanistic modeling of the break-away regime in this alloy. We think that the large tensile cracks which appear in the outer part of the oxide scales in a later stage are a consequence of the volume increase caused by the shear crack formation.

Ferritic/martensitic (f/m) steels are candidates as materials for structural components in e.g. accelerator driven systems. The oxide scales on f/m steels consist in general of two sublayers namely a magnetite (outer part) and a Fe/Cr spinel (inner part) [37,38]. The magnetite is known to grow by outside oxidation, as the oxygen diffusivity in the bulk is much lower than the iron diffusivity [39]. The spinel sublayer is viewed to grow by interface oxidation. This means, that our model for a duplex scale can be applied to oxidizing tubes of f/m steels. Observations on decohesion effects at the interface between the two sublayers and on spalling of whole parts of the oxide layer are reported in refs. [37,38]. It could be that all these mechanical effects are mainly due to thermal cycling, especially due to the temperature change occurring upon unloading of the samples. Decohesion at the interface of the two sublayers could, for example, be due to the difference in the thermal expansion coefficients of magnetite and Fe/Cr spinel. But it could also be that some mechanical effects have occurred at steady-state conditions. It is difficult to conclude on this, as in the majority of the tests no detailed information on the temperature history is given. Only a few results of post test examinations are included in these reports. Therefore we do not know, whether all aspects of mechanical effects in the oxide scale were really documented. If the oxidation strain tensor is uniaxial, the stress state in the duplex scale at temperature would be relatively low with tensile stresses in the Fe/Cr spinel and compressive stresses in the magnetite sublayer and it is doubtful whether spalling effects could occur at steady-state conditions for oxide scale thickness values of less than about 30 µm.

In ref. [40] observations on mechanical effects on duplex scales on 9% Cr steels and AISI 316 are reported. Only the magnetite subscale was found to spall, whereas the Fe/Cr spinel remained attached to the metallic substrate.

The situation of experimentally determined growth stresses in NiO, Cr_2O_3 and Al_2O_3 scales was reviewed in ref. [6] Huntz and Schütze distinguished between geometrically induced stresses and intrinsic growth stresses. In the light of our model geometrically induced

stresses would be caused by the oxidation strain component acting orthogonal to the surface of the specimens and intrinsic growth stresses by the lateral components in the oxidation strain tensor. The authors concluded that that the growth stresses in these oxide scales are of small amplitude compared to thermal stresses probably on account of stress relaxation at high temperature. The values of the growth stresses range from up to 1365 MPa for NiO scales to about -400 MPa for Al_2O_3 scales. In [41] were also included measurements of lateral strains of ferritic steel specimens oxidized at 800°C, which had been taken from [18]. In ref. [6] are also reported values of residual stresses at room temperature. Especially, in alumina scales very high compressive stresses have been measured (-2500 to -5700 MPa). This shows that oxide scales can bear eventually very high compressive stresses.
The results of deflection tests on samples with a Ni-20Cr alloy are reported in ref. [42]. For the calculation of growth stresses a finite-element code was used assuming an anisotropic oxidation strain. For the lateral components a value of 0.005 was taken. Visco-plastic behavior was permitted for both the NiO film and the metal substrate [42]. The calculated stresses in the oxide film were mainly compressive with the highest absolute values occurring at the beginning of an oxidation cycle. These maximum values range between -600 and -300 MPa. With the help of our simplified formula (58) and the data given in ref. [42] we have calculated a value of -1020 MPa for the elastic hoop stress in the NiO film.
Length increases of up to 1% for non-deformed specimens and of up to about 3.5% for mechanically deformed specimens are reported in ref. [18]. The authors concluded that the elastic intrinsic growth stress level in the chromia scale would have been at -2800 MPa for the non-deformed samples and at -9800 MPa for the mechanically deformed samples. These stress levels have not been reached as there occurred scale detachment. It is not possible to deduce directly the lateral oxidation strains from the measurements of ref. [18]. It was the total lateral strain, what has indeed been measured and this total strain is a superposition of different strain contributions from oxidation, elastic, and inelastic behavior of the scale:

$$\varepsilon_z^{tot} = e_z^{ox} + \varepsilon_z^{el} + \varepsilon_z^{inel} \tag{70}$$

The elastic strain is determined by the growth stress in the scale but the inelastic contribution is also a function of this stress. As cylindrical test specimens had been used, the growth stress in the scale consisted of a geometrical and an intrinsic contribution. Assuming that there is no inelastic strain, we have done studies with our model and we have found that the total axial strain increases linearly with the scale thickness.

Residual stresses in NiO bi-layers at room temperature were measured in [43]. It was found that a complex stress state can exist in such a duplex scale with a compressive stress in the inner sublayer of about -950 MPa and a tensile stress in the outer sublayer. The fact that the measured residual stress does not depend on the oxidation temperature is rather astonishing. The calculation of the growth stresses from the residual stresses needs the thermal expansion coefficients of the two different modifications of NiO. Assuming that both modifications have the same thermal expansion coefficients and using data on the difference ($\Delta\alpha = \alpha_{Ni} - \alpha_{NiO}$) known from the literature [41] we have estimated the thermal stress to range between about -600 and -850 MPa, as the oxidation temperatures were between 900 and 1200°C. That means the intrinsic growth stress in the inner layer should range between about -100 and -350 MPa. The geometrical growth stress in thin foils should be rather small.

Thus, we have a strong hint on the existence of lateral components in the oxidation strain tensor of NiO.

Very high intrinsic tensile growth stresses (1365 MPa) in NiO scales on thin foils have been reported in ref. [41].The measurements have been done with the help of an X-ray diffraction method following the whole temperature history of the tests. We have made sensitivity studies with our model and found that tensile intrinsic growth stresses can (only) be explained with the help of negative lateral oxidation strain components.

In order to estimate the magnitude of the lateral oxidation strain components we have derived the following simplified formula for the intrinsic growth stresses in the scale on a thin foil under the assumption that both lateral components are equal:

$$\sigma_y^{i.g.s.} = -\frac{E^f}{1-\nu_f} \cdot \frac{1}{1+\frac{h \cdot \Phi}{s_{me}} \cdot \frac{1-\nu_{me}}{1-\nu_f} \frac{E_f}{E_{me}}} \cdot e_x^{ox} \qquad (71)$$

$$\sigma_x^{i.g.s.} \approx \sigma_y^{i.g.s.}$$

x, y : coordinates in the plane of the oxide scale

With the help of this formula we could estimate that the lateral oxidation strain components should range between about -0.004 and -0.005, if the intrinsic growth stress in the NiO scale is at about 1360 MPa as reported in ref. [41]. For the growth stresses of ref. [43] we would estimate the lateral strain components to be in the order of 0.001.

There are more data on growth and residual stresses in NiO scales and corresponding references given in [6]. The growth stresses, for example, range between -90 and 1365 MPa. The reasons for this big scatter are not clear. It could be due to the fact that different types of mono- or bi-layered scales of NiO can be formed or due to problems of the methods of measurement or to incorrect values of the thermal stresses.

Rhines and Wolf [2] proposed as an explanation for their observations on the oxidation of Ni specimens a model based on the deposition of new oxide upon the internal boundaries of pre-existing columnar oxide grains leading to the production of compressive scale stresses. Such a mechanism can certainly be described with the help of lateral components in the oxidation strain tensor as the action of the new oxide goes into azimuthal and into the axial direction. The model of Rhines and Wolf would, of course, suggest positive values for the lateral oxidation strain components.

In ref. [44] are reported evolutions of growth stresses in Al_2O_3 scales obtained from the measurement of bending of thin strips. The tests were done at 1000°C. As in thin strips the geometric growth stresses should be small, we think that essentially the intrinsic growth stresses have been measured. The growth stresses were always compressive. At the beginning of the oxidation process the growth stresses rose quickly up to a maximum value of up to -700 MPa, afterwards stress relaxation effects could be seen. The steady-state

values ranged between -50 and -400 MPa. With the help of (71) we can again estimate the magnitude of the lateral oxidation strain components and obtained in this way values of up to 0.0017.

More recent measurements of growth stresses in Al_2O_3 scales at temperature on FeCrAl based alloys and on NiAl specimens done with different in situ X-ray diffraction methods are reported in refs. [45-47]. The obtained results are very disparate, ranging from rather high compressive stresses in ref. [47] (-1 GPa) to rather high tensile stresses in [45] with values of up to 1 - 1.2 GPa in the early stage of the oxidation with a subsequent decrease for oxidation temperatures above about 1100°C. But also very low growth stresses have been measured [46]. The values of lateral oxidation strain components would accordingly range between about -0.005 and 0.0045.

The decrease of the growth stresses after the initial maximum can be due either to stress relaxation mechanisms or due to relief of epitaxial constraints or both [44]. The lattices of metal alloys and surface oxides are usually dissimilar. Hence, the nucleation and growth of oxides may be accompanied by the development of epitaxial stresses [48]. The epitaxial constraint can be modeled with the help of lateral oxidation strain components. Once an oxide scale grows, the epitaxial constraints are reduced. This would then mean that the lateral oxidation strain components would diminish with increasing oxide scale thickness. This situation could be described with the help of some simple modification of our model. Epitaxial constraints can eventually lead to tensile growth stresses, a possibility which should not be dismissed.

All our estimates of lateral oxidation strain components are based on relation (71). But this relation relates the elastic stresses to the strain, whereas the experimental values of growth stresses are suspected to include some stress relief. Hence, the true values of the lateral oxidation strain components may be considerably higher than our estimated values. In this way the values of growth stresses obtained with an elastic model based on the true values of the oxidation strains would then also be distinctly higher than experimental values.

The experimental results for growth stresses reported in [6] were all for oxidations at high temperatures, where stress relaxation mechanisms are probably most effective. But in accelerator driven systems the maximum foreseen temperature will be at 550°C. If the oxidation temperature is below the transition temperature for oxide deformation, purely elastic behavior of the oxide scale before cracking is to be expected [48]. Then relief of growth stresses can occur by tensile or shear cracking or by scale detachment or can also occur via ‘pseudo-plasticity’ [6]. This is due to a mechanism consisting of continuous micro-crack formation along oxide grain boundaries with superimposed healing of these micro-cracks by the oxidation process.

9. Conclusions

The Pilling-Bedworth ratio determines the volume increase or decrease upon oxidation. Whether growth stresses are generated in the oxide scale and in the metallic substrate depends on the geometrical structure of the component and on the structure of the oxidation strain tensor. In case of a flat structural component we would, except for end effects, obtain no growth stresses for a uniaxial oxidation strain tensor. But so-called geometrically induced growth stresses would be generated in curved structural components. The lateral components of the oxidation strain tensor are responsible for the so-called intrinsic growth stresses. Based on experimental values of intrinsic growth stresses we could estimate the magnitude of these lateral strain components. Evidence for the action of lateral oxidation strains seems to be rather convincing for the case of Zry exposed to air, a problem which is of some importance in Light Water Reactor safety as there are scenarios of air ingress.

Future work on the newly developed model will tend to investigate creep in the metallic substrate and in the oxide film and study the effects due to thermal cycling. In order to deal with the important stress relief mechanisms in the oxide scale like cracking (tensile or shear), spalling and scale detachment must have recourse to the methods of fracture mechanics. But we need in any case the stress values of the extended visco-elastic model as a basis for the analysis. Thermal stresses are now relatively well understood. A similar understanding of the mechanisms, character and effects of growth stresses has not been attained. The newly developed visco-elastic model for oxidation growth stresses should be helpful in this respect. We consider it as a valuable tool and a starting point for the analysis of stress situations in oxidizing tubes. Especially, the role of lateral components of the oxidation strain tensor has been highlighted.

References

[1] P.D. Dankov and P.V. Churaev, Doklady Akad. Nauk. SSSR 73, 1221-1224, (1950)
[2] F.N. Rhines and J.S. Wolf, Metal Transactions 1, 1701-1710, (1970)
[3] J. Stringer, Corrosion Science 10, 513-543, (1970)
[4] F. H. Stott and A. Atkinson, Materials at High Temperatures 12, 195, (1994)
[5] H. E. Evans, International Materials Reviews 40, 1-40, (1995)
[6] A. M. Huntz and M. Schütze, Materials at High Temperatures 12, 151-161, (1994)
[7] E. Mitchell, D.A. Voss and E.P. Butler, Materials Science 17, 1825-1833, (1982)
[8] P. Hancock and J. R. Nicholls, Materials at High Temperatures 12, 209-219, (1994)
[9] W. Christl, A. Rahmel and M. Schütze, Oxidation of Metals 31, 1-34, (1989)
[10] J.D. Nodden, C.J. Knights and M.W. Thomas, British Corrosion Journal 3, 47-55, (1968)
[11] V.K. Tolpygo and D.R. Clarke, Oxidation of Metals 49, 187-212, (1998)
[12] M. M. Nagl, S. R. J. Saunders and V. Guttmann, Materials at High Temperatures 12, 163-168, (1994)
[13] Y. Rosenband, A. Gany and Y.M. Timmat, Oxidation of Metals 43, 141-156, (1995)
[14] W. Przybilla and M. Schütze, Oxidation of Metals 58, 103-145, (2002)

[15] M. Schulte and M. Schütze, Oxidation of Metals 51, 55-77, (1999)
[16] M. I. Manning, Corrosion Science 21, 301-316, (1981)
[17] C. H. Hsueh and A. G. Evans, Journal of Applied Physics 54, 6672-6686, (1983)
[18] M. Schütze, Oxidation of Metals 24, 199-232, (1985)
[19] H.L. Bernstein, Metallurgical Transactions 18A (1987) 975-985
[20] V. Rosenband and A. Gany, Corrosion Science 37 (1995) 1991-2001
[21] M. Schütze, Oxidation of Metals 44, 29-61, (1995)
[22] C. Petersen, Report KfK 3469 (1983)
[23] H. Steiner, Report FZKA 6737 (2002)
[24] H.E. Evans, Int. Mat. Rev. 40 (1995) 1-40
[25] H. Steiner, J. Konys: Stresses in oxidized claddings and mechanical stability of oxide scales, FZKA 7191 (2006)
[26] J. Armitt, D.R. Holmes, M.L. Manning, D.B. Meadowcroft, and E. Metcalfe, EPRI Report N4 FP-686 (1978)
[27] C. Petersen, KfK Report 3469 (1983)
[28] S. Osgerby, Mat. High Temp. 17(2) (2000) 307-310
[29] J. Robertson, M.I. Manning, Mat. Sc. Technol., 6 (1990) 81-91
[30] M. Schütze, Ox. Met. 44 (1995) 29-61
[31] E.B. Evans, N: Tsangarakis, H. B. Probst, N.J. Garibotti, Proceedings of the Symposium of the Metallurgical Society AIME, Boston, 342-349 (1972)
[32] S. Leistikow, H. von Berg, unpublished (1982)
[33] B. Burton, Journal of Nuclear Materials 113 (1983) 172-178
[34] B. Burton, A.T. Donaldson, and G.L. Reynolds, Zirconium in the Nuclear Industry, Fourth Conference ASTM STP 681 (1979) 561-585
[35] M. Parise, O. Sicardy, G. Cailletaud, Journal of Nuclear Materials 256 (1998) 35-46
[36] G. Schanz, S. Leistikow, Proc. 8th Int. Congr. on Met. Corr., Mainz, Sept. 6-11, 1981 Frankfurt a.M.: Dechema 1981. Voll.II S. 1712-17 (1981)
[37] J. Zhang, N. Li, Y. Chen, A.E. Rusanov, Journal of Nuclear Materials 336, 1-10, (2005)
[38] A. Heinzel, FZKA 6823 (2003)
[39] J.E. Castle and P.L. Surman, Journal of Physics and Chemistry 75, 632-634, (1969)
[40] J. Robertson, M.I. Manning, Materials Science and Technology 6, 81-91, (1990)
[41] J.G. Goedjen, J.H. Stout, Q. Guob and D.A. Shores, Materials Science and Engineering: A, 177, 115-124, (1994)
[42] A.M. Huntz, G. Calvarin Amiri, H.E. Evans, and G. Cailletaud, Oxidation of Metals 57 (2002) 499-521
[43] T. Ueno, Trans. Japanese Institute of Metal 15, 167-173, (1974)
[44] D. Delaunay, A.M. Huntz and P. Lacombe, Corrosion Science 20, 1109-1117, (1980)
[45] P.F. Tortorelli, K.L. More, E.D. Specht, B.A. Pint and P. Zschack, Materials at High Temperatures 20(3), 303-309, (2003)
[46] E. Schumann, C. Sarioglu, J.R. Blachere, F.S. Pettit, and G.H. Meier, Oxidation of Metals 53, 259-273, (2000)
[47] C. Sarioglu, J.R. Blanchere, F.S. Pettit, and G.H. Meier, Microscopy of Oxidation 3, 41, S.B. Newcomb and J.A. Little, eds (The Institute of Materials, London, 1997),
[48] G.W. Groves, Proc. British Ceramic Society 15, 103-111, (1970)
[49] P. Hancock and R. C. Hurst, Adv. in Corrosion Science and Technology 4, Plen. Press, N. Y., 1- 84, (1974)